



Interfacial features of TiAl alloy/316L stainless steel joint brazed with Zr–Cu–Ni–Al amorphous filler metal

Hong-gang DONG, Run-ze ZHANG, Yue-qing XIA, Xiao-hu HAO, Peng LI

School of Materials Science and Engineering, Dalian University of Technology, Dalian 116024, China

Received 15 June 2020; accepted 28 January 2021

Abstract: TiAl alloy and 316L stainless steel were vacuum-brazed with Zr–50.0Cu–7.1Ni–7.1Al (at.%) amorphous filler metal. The influence of brazing time and temperature on the interfacial microstructure and shear strength of the resultant joints was investigated. The brazed seam consisted of three layers, including two diffusion layers and one residual filler metal layer. The typical microstructure of brazed TiAl alloy/316L stainless steel joint was TiAl alloy substrate/ α_2 -(Ti₃Al)/AlCuTi/residual filler metal/Cu₉Zr₁₁+Fe₂₃Zr₆/Laves-Fe₂Zr/ α -(Fe,Cr)/316L stainless steel substrate. Discontinuous brittle Fe₂Zr layer formed near the interface between the residual filler metal layer and α -(Fe,Cr) layer. The maximum shear strength of brazed joints reached 129 MPa when brazed at 1020 °C for 10 min. The diffusion activation energies of α_2 -(Ti₃Al) and α -(Fe,Cr) phases were –195.769 and –112.420 kJ/mol, respectively, the diffusion constants for these two phases were 3.639×10^{-6} and 7.502×10^{-10} $\mu\text{m}^2/\text{s}$, respectively. Cracks initiated at Fe₂Zr layer and propagated into the residual filler metal layer during the shear test. The Laves-Fe₂Zr phase existing on the fracture surface suggested the brittle fracture mode of the brazed joints.

Key words: vacuum brazing; dissimilar joining; Zr-based amorphous filler metal; intermetallic compound; growth kinetics

1 Introduction

Titanium alloy possesses prominent performance, such as high specific strength, low density and high temperature resistance. However, the high cost limits the wider application of titanium alloy. Stainless steel has advantages such as low cost, high corrosion resistance and good machinability [1]. The hybrid joint of titanium alloy and stainless steel could combine both advantages of these two materials, therefore, it has extensive applications in aerospace, nuclear industries and energy industries [2,3]. However, it is hard to obtain reliable joints between titanium alloy and stainless steel due to the differences in thermo-physical properties and chemical compatibility [4].

Various welding methods were used to join

titanium alloy and stainless steel, such as solid-state welding [5,6], fusion welding [7,8] and brazing [9–13]. In comparison, brazing has advantages in low welding residual stress, flexible joint type and low welding temperature. Ag-based and Ti-based filler metals were most widely used to braze titanium alloy and stainless steel. Ag-based filler metals have good compatibility with titanium alloy but the high cost is the largest barrier for wider applications. Joints brazed with Ti-based filler metal have excellent resistance of corrosion and elevated temperature [9], but brittle Ti–Fe intermetallic compounds (IMCs) are easily generated in the brazed seam and deteriorate the mechanical properties of resultant joints.

LEE et al [10–12] used Ag–Cu filler metal and Ag interlayer to braze pure Ti(Gr2) and UNS S31254 stainless steel. It was found that the Ag

interlayer could effectively prevent the formation of brittle TiFe and TiFe₂ IMCs, and due to the generation of ductile TiAg phase, the maximum tensile strength of the resultant joint reached 410 MPa. Moreover, the addition of Pd element into the filler metal improved the corrosion resistance of joints. NODA et al [13] brazed TiAl alloy and AISI 4340 stainless steel with Ti–Cu–Ni filler metal, and detected massive brittle Ti-based IMCs, such as TiC and Ti(Fe,Al) in the brazed seam. The tensile strengths of joint were 210 MPa at room temperature and 255 MPa at 500 °C.

Benefited from the fast development of rapid cooling technique, amorphous alloy foil could be prepared conveniently. Amorphous filler metals could be easily manufactured into foil with neat appearance. Zr-based alloy has good amorphous forming ability and similar characteristics with Ti-based alloy. In order to combine low cost of filler metal and good metallurgical compatibility between the filler metal and base metal, Zr–Cu–Ni–Al amorphous filler metal was developed to braze TiAl alloy and 316L stainless steel (316L SS) in this work. The influence of brazing parameters on the interfacial microstructure and shear strength of the brazed joints was investigated.

2 Experimental

Zr–Cu eutectic alloy was used as the base of filler metal because of its good amorphous forming ability. Based on the cluster approach proposed by DONG and DONG [14], the alloying elements were chosen according to the low mixing enthalpy, and the new alloy can be designed through the similar element replacement method. Ni and Al could be considered as similar elements to Cu due to their low mixing enthalpy calculated by TAKEUCHI and INOUE [15]. In this way, the Zr–Cu–Ni–Al filler metal was designed, and the composition of the filler metal was expressed as Zr–50.0Cu–7.1Ni–7.1Al (at.%). Rapid cooling technique was used to prepare the amorphous filler metal. First, the raw materials of Zr, Cu, Al, and Ni with the purity of 99.99% were exactly weighed, then the mixed raw materials were arc melted at least four times to produce homogeneous alloy ingot. Finally, the filler metal foil was fabricated by rapid cooling process, and the resultant filler metal foil was ~5 mm in width and ~100 μm in thickness.

316L stainless steel (Fe–16.8Cr–10.4Ni–2.0Mo, wt.%) and TiAl alloy (Ti–26.8Al–15.6Nb, wt.%) were employed as the base metals. The base metals were cut into the dimensions of 15 mm × 10 mm × 4 mm and 5 mm × 5 mm × 4 mm by wire cutting method, respectively. The faying surfaces of base metals were ground with 600# grit SiC paper and then ultrasonically cleaned in acetone for about 10 min.

The base metals and filler metal were assembled as shown in Fig. 1(a). The brazing experiment was conducted in a vacuum brazing furnace under a vacuum degree of 5×10^{-3} Pa. Figure 1(b) shows the heating process of the brazing experiment. The samples were heated to 800 °C at a rate of 20 °C/min, and held for 10 min at 250 and 800 °C, respectively. Then, the samples were heated to the brazing temperature and held for the chosen brazing time, and finally cooled down in the furnace. The brazing temperature and brazing time were set as the range of 990–1050 °C and 5–40 min, respectively. After brazing, the cross sections of the joints were ground with SiC paper from 200# to 5000# grit, then polished with 1.5 μm diamond polishing paste to examine the influence of brazing parameters on microstructure of the joints.

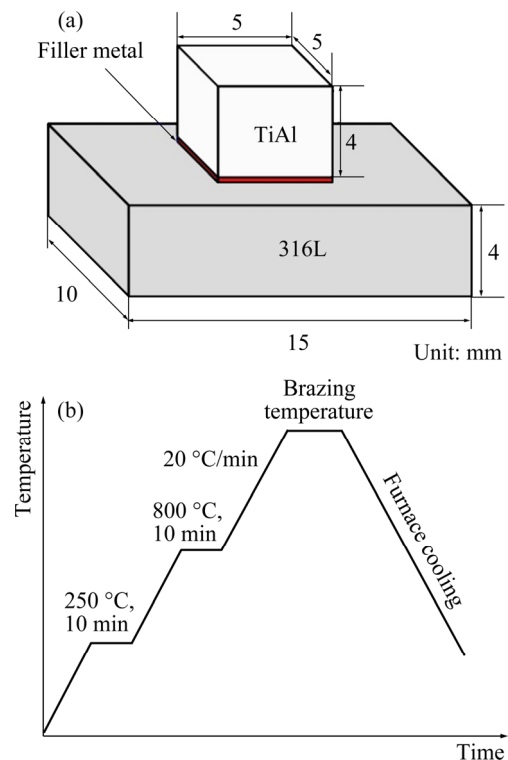


Fig. 1 Assembly of brazed samples (a) and time-temperature heating curve for brazing process (b)

The microstructure and thermal property of the filler metal were measured by an X-ray diffraction device (XRD, Empyrean, Netherlands) and a differential thermal analysis device (DTA, TA Q600, America), respectively. The microstructure and elemental distribution of brazed seam were examined by electron probe micro-analyzer (EPMA, JXA-8530F Plus, Japan). The shear test of brazed joints was conducted by a universal testing machine (DNS-100, China) with a test speed of 0.5 mm/min. The sample and fixture were assembled as shown in Fig. 2. The fracture morphology and chemical composition were analyzed by a scanning electron microscope (SEM, ZEISS-SUPRA55, Germany) with an energy dispersive spectroscopy (EDS, Oxford Instruments, UK).

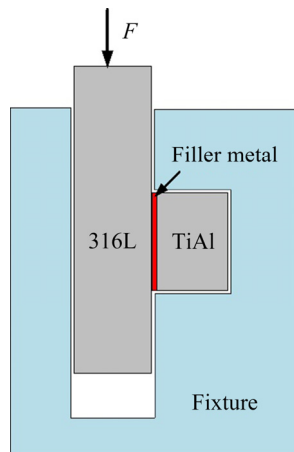


Fig. 2 Assembly of brazed sample and fixture

3 Results and discussion

3.1 Characterization of filler metal

The XRD pattern and DTA curve of the filler metal are shown in Fig. 3. There is no diffraction peak corresponding to crystallization phases but only one broad diffraction peak, revealing the amorphous structure of the filler metal. The solidus temperature (T_m) and liquidus temperature (T_l) of the filler metal are 925 and 965 °C, respectively. Generally, the brazing temperature should be slightly higher than the liquidus temperature of the filler metal. As a result, the brazing temperature in this study is determined as 990–1050 °C.

3.2 Elemental distribution

The elemental distribution in the joint brazed at 990 °C for 10 min is shown in Fig. 4. There are

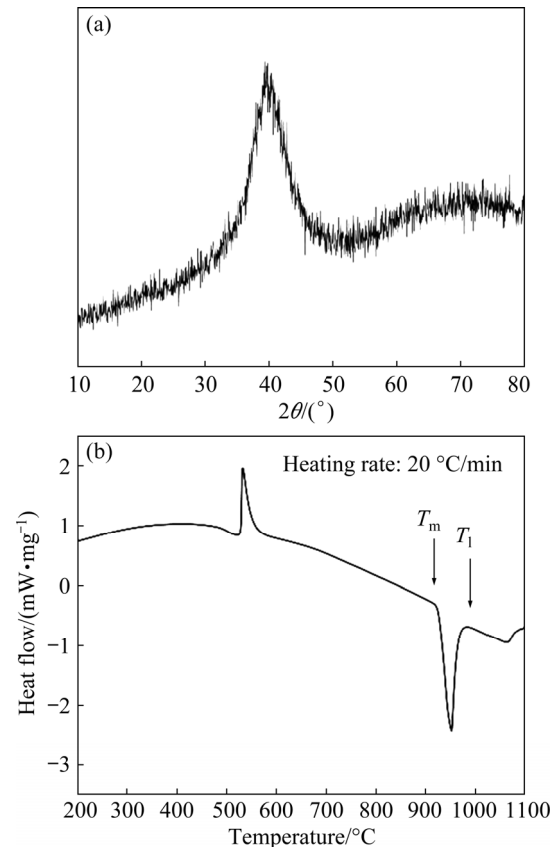


Fig. 3 XRD pattern (a) and DTA curve (b) of Zr–Cu–Ni–Al filler metal

three visible layers marked as I, II and III in the brazed seam, as shown in the backscattered electron image (BEI). The boundaries of Layer II are irregular, which could be the interface between the base metals and liquid filler metal. Three different phases exist in Layer II, i.e., white phase, deep-grey island phase, and light-grey phase near Layer III. Little Ti and Fe diffused to other side of the seam, revealing that the formation of brittle Ti–Fe IMCs was restrained. Layer II mainly consisted of Zr, Cu, Al, and Ni elements, so it could be deduced as the residual filler metal. Cu is rich in the deep-grey phase but poor in the light-grey phase. The distribution of Al in Layer I reflects that Al diffuses from TiAl substrate to the brazed seam and consequently thick α_2 -(Ti₃Al) phase may form here. Zr mainly exists in Layer II, especially in the white phase. There is barely diffusion of Zr between the base metal and filler metal. Ni attenuation and Cr enrichment occur in the Layer III near 316L SS, suggesting that the uphill diffusion of Cr occurred here. It has been reported that the diffusion of Ti into 316L SS would weaken the activity of Cr, and

the diffusion of Cr is driven by the activity gradient rather than the concentration gradient [16].

The microstructure and line analysis results for the typical joint brazed at 990 °C for 10 min are

shown in Fig. 5, and the corresponding quantitative composition results are listed in Table 1. The result in Fig. 5(b) indicates that most of Ti exists in TiAl substrate and Layer I; the content of Al decreases

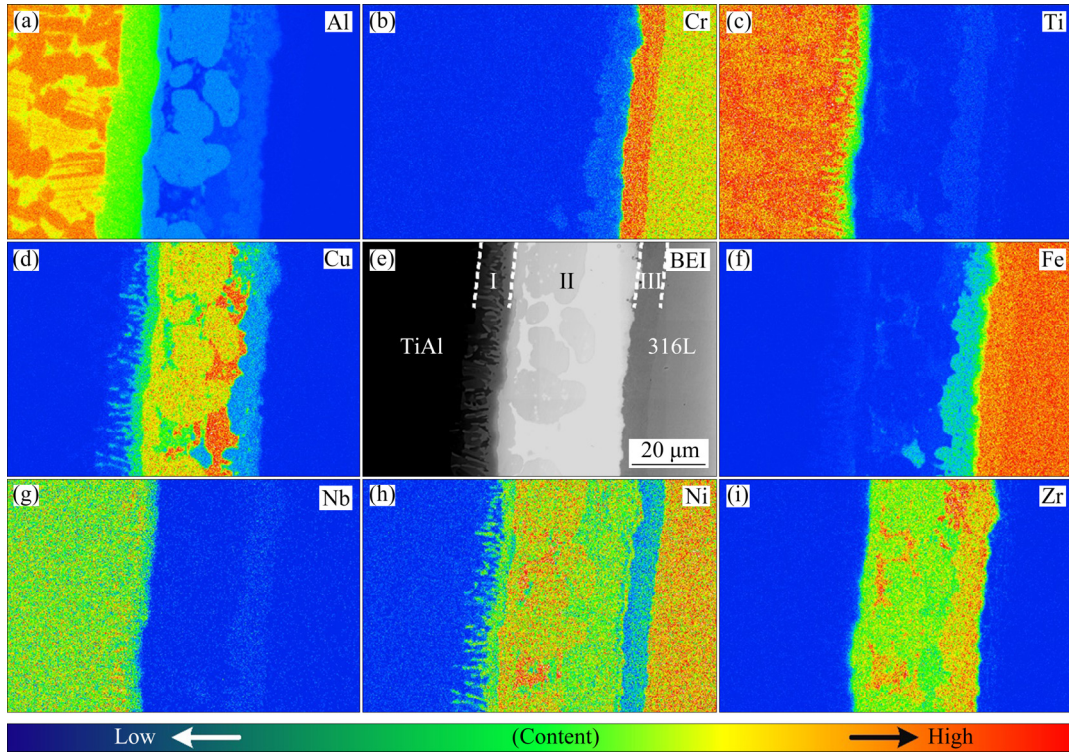


Fig. 4 Elemental distribution maps of joint brazed at 990 °C for 10 min: (a) Al; (b) Cr; (c) Ti; (d) Cu; (e) Backscattered electron image of brazed seam; (f) Fe; (g) Nb; (h) Ni; (i) Zr

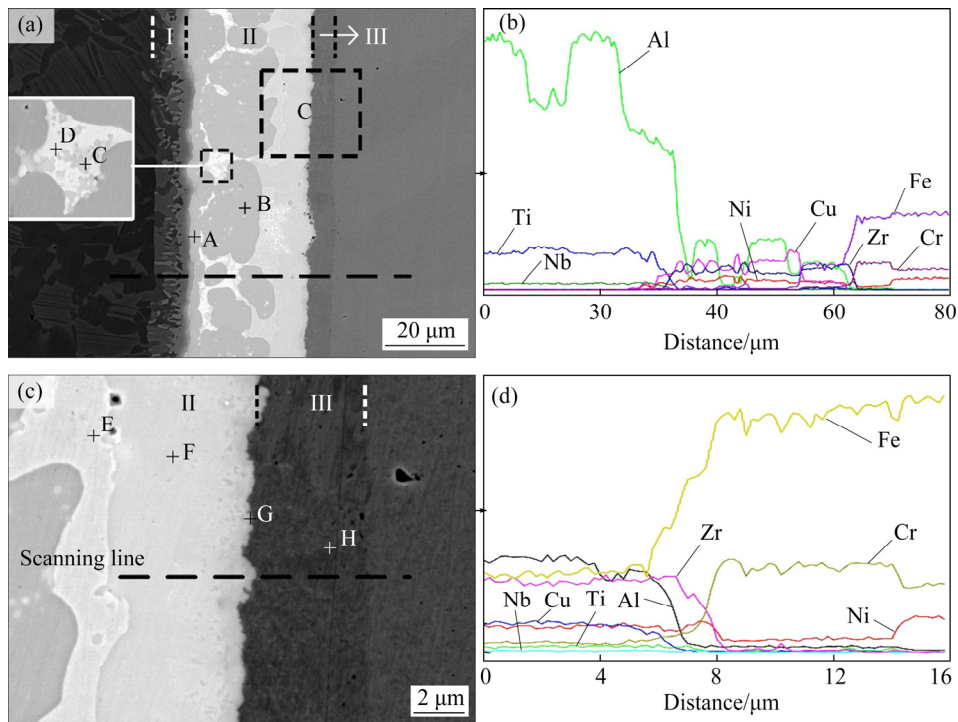


Fig. 5 Typical microstructures (a, c) of joint brazed at 990 °C for 10 min and corresponding analysis results (b, d): (a, b) Cross section; (c, d) Magnified view of interface near 316L stainless steel

from TiAl substrate to 316L SS base metal and the lowest point locates in the white phase; Cu has an opposite changing trend compared with Zr. In addition, an Al-dilution layer exists in Layer I. It could be α_2 -(Ti₃Al) phase [17] due to the diffusion of Al to the brazed seam. Simultaneously, a Ni-poor layer with the thickness of 7–8 μm can be seen in Fig. 5(d).

AlCuTi phase (Location A) formed in the Layer I due to the diffusion of Cu from filler metal to TiAl substrate, according to the Al–Cu–Ti ternary phase diagram [18]. The phase at Location H was determined to be α -(Fe,Cr) solid solution, based on the Fe–Cr binary phase diagram [5]. The discontinuous layer (Location G) near Layer III is mainly composed of Fe and Zr, and their composition ratio is near 2:1, suggesting that Laves Fe₂Zr phase with AB₂ type formed according to the Fe–Zr binary phase diagram [5]. The class of AB₂ Laves phase usually crystallizes with the cubic C15 structure which is face-centered cubic (FCC) [18]. Thus, the non-coherent or half-coherent interface possibly forms between Laves phase and body-centered cubic (BCC) α -(Fe,Cr) phase, resulting in the large elastic distortion energy at the Laves phase/ α -(Fe,Cr) interface and producing a weak point at this interface [19].

3.3 Microstructure evolution and growth kinetics of diffusion zone

Figure 6 shows the microstructure of joints under different brazing conditions. It can be seen that the brazing temperature has a greater effect on the width of brazed seam than brazing time. The diffusion mechanism in the brazed seam is close to the steady state diffusion. According to the Fick's

first law, we can obtain equations as follows:

$$J = -k \frac{dc}{dx} \quad (1)$$

$$k(T) = k_0 \exp\left(\frac{-Q}{RT}\right) \quad (2)$$

where J is the amount of diffused material in unit time and unit area, k is the diffusion coefficient, k_0 is the diffusion constant, dc/dx is the concentration gradient, Q is the diffusion activation energy, R is the gas constant, and T is the brazing temperature. The amount of diffused material is linear in time and exponential correlation in temperature. Increasing the brazing time could homogenize the microstructure in brazed seam.

The formation and thickening of Layer I (α_2 -(Ti₃Al)) and Layer III (α -(Fe,Cr)) are attributed to the diffusion of Al from TiAl and Cr from 316L SS, so the relation between the thickness of diffusion zone and brazing time is parabolic [20] and it can be described as follows:

$$W^2 = kt \quad (3)$$

where W is the thickness of diffusion layer, and t is the brazing time. The fitting curves based on the thickness data in Table 2 are shown in Fig. 7. The slopes of curves in Fig. 7 are calculated and the relation between diffusion coefficient and temperature follows the Arrhenius equation [21]:

$$k = k_0 \exp\left(\frac{-Q}{RT}\right) \quad (4)$$

The value of k is related to T , so k_0 and Q could be calculated and their relation could be described as

Table 1 EPMA analysis results of different locations in Fig. 5 (at.%)

Location	Ti	Zr	Cu	Ni	Fe	Cr	Nb	Al	Possible phase
A	30.2	1.8	21.3	5.5	2.7	0.14	4.7	32.5	AlCuTi
B	0.5	24.6	45.4	8.3	0.8	–	–	18.3	AlCu+ZrCu
C	2.5	45.4	23.4	5.0	3.8	–	–	13.5	CuZr+Al ₂ Zr ₃
D	3.5	37.2	38.2	13.4	3.0	–	–	1.9	Residual filler metal
E	0.5	21.2	59.9	6.7	3.1	0.3	–	6.0	Cu ₈ Zr ₃
F	4.1	30.6	19.7	7.9	21.6	2.5	0.4	8.3	Cu ₉ Zr ₁₁ +Fe ₂₃ Zr ₆
G	3.5	23.0	–	6.7	55.1	7.6	–	–	Laves-Fe ₂ Zr
H	0.7	–	0.3	3.2	69.4	25.7	–	0.4	α -(Fe,Cr)

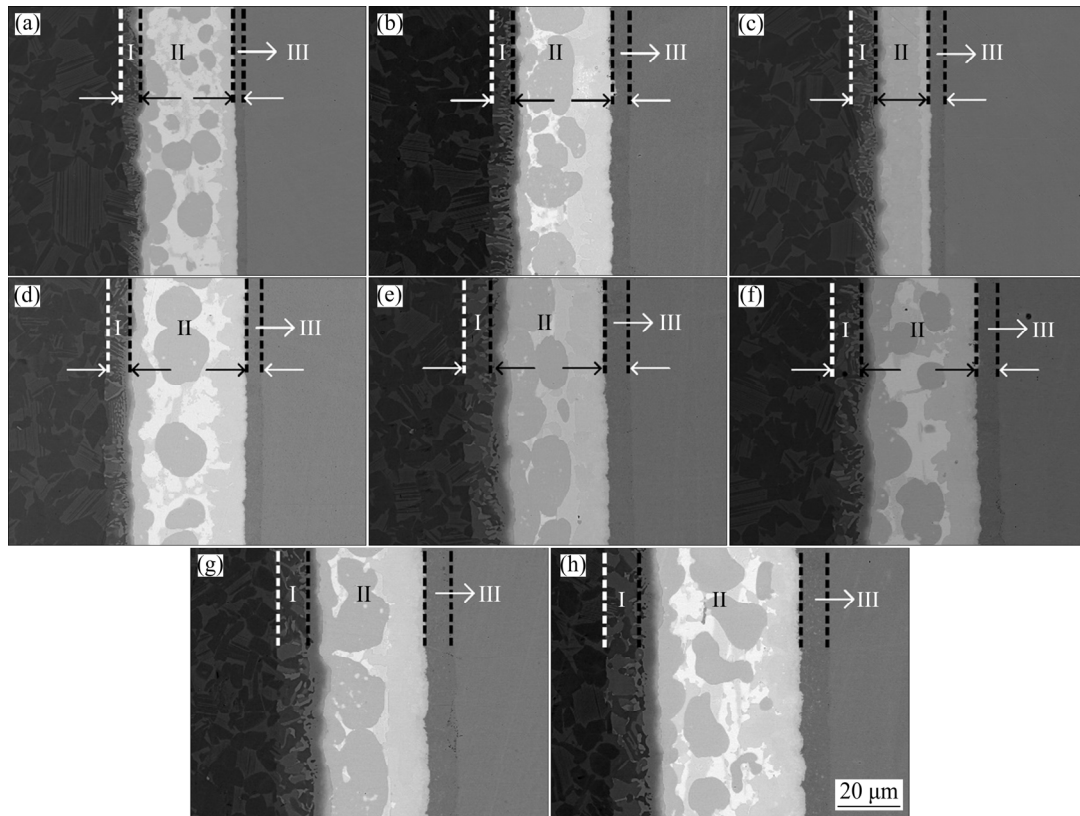


Fig. 6 Influence of brazing parameters on microstructure of brazed joints: (a) 990 °C, 5 min; (b) 990 °C, 10 min; (c) 990 °C, 20 min; (d) 1020 °C, 5 min; (e) 1020 °C, 10 min; (f) 1020 °C, 20 min; (g) 1020 °C, 40 min; (h) 1050 °C, 10 min

Table 2 Thickness of reaction layer in joints brazed with different brazing parameters

Reaction layer	Temperature/°C	Thickness/μm		
		5 min	10 min	20 min
α_2 -(Ti ₃ Al)	990	6.46	7.03	8.21
	1020	7.23	8.77	9.75
α -(Fe, Cr)	990	3.48	5.63	5.51
	1020	5.10	7.74	7.08

$$W = 3.639 \times 10^{-6} \sqrt{t} \exp\left(\frac{-195.769}{RT}\right)$$

for α_2 -(Ti₃Al) layer and

$$W = 7.502 \times 10^{-10} \sqrt{t} \exp\left(\frac{-112.420}{RT}\right)$$

for α -(Fe,Cr) layer. It can be found that α -(Fe,Cr) layer is easier to form and α_2 -(Ti₃Al) layer has a high thickening rate.

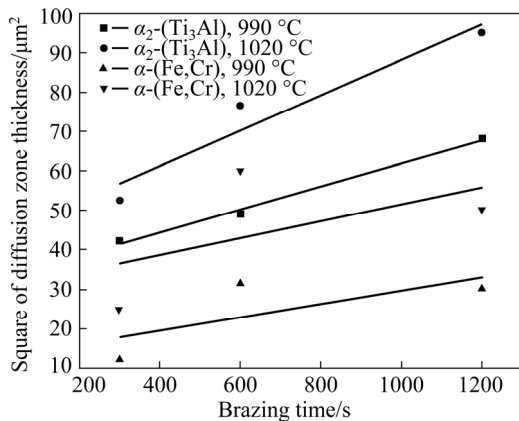


Fig. 7 Relationship between thickness of diffusion zone and brazing time

3.4 Shear strength

The average shear strength of brazed joints is shown in Fig. 8. With increasing the brazing temperature and brazing time, the joint shear strength first increased and then decreased. The peak shear strength reached 129 MPa when brazed 1020 °C for 10 min. Low brazing temperature or short brazing time constricted the interdiffusion of alloying elements between base metals and filler metal, therefore, the interfacial diffusion and reaction were insufficient, resulting in the low bonding strength of the brazed joints. However, the low shear strength of the joints brazed at high

brazing temperature or longer brazing time was caused by the formation of the discontinuous brittle Fe_2Zr layer.

3.5 Fracture morphology

The typical fracture morphology of the joint brazed at 1020 °C for 10 min is shown in Fig. 9. The corresponding EDS results of feature locations on the fracture surface are listed in Table 3. Cleavage facets and voids without any dimple can be seen on the fracture surface, revealing the brittle

fracture mode of the brazed joints. Fe_2Zr phase is the major phase that was detected on both sides of fracture surface, demonstrating once again that the brittle Fe_2Zr layer is the weak point of the brazed joints as mentioned earlier. According to the EDS analysis results at locations B and D, Fe_2Zr phase mainly distributed in the voids of joints. $\text{Cu}_9\text{Zr}_{11}$ and $\text{Fe}_{23}\text{Zr}_6$ phases are detected around the secondary cracks on the fracture surface (location C) on TiAl side, and $\alpha\text{-(Fe,Cr)}$ is detected on the fracture surface on 316L SS side.

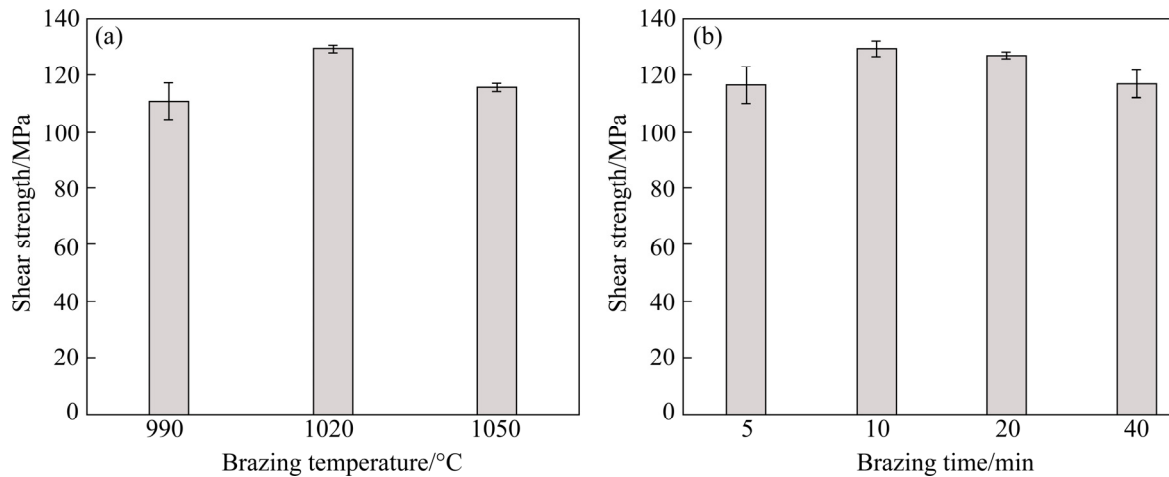


Fig. 8 Shear strength of joints brazed at different brazing temperatures for 10 min (a), and at 1020 °C for different brazing time (b)

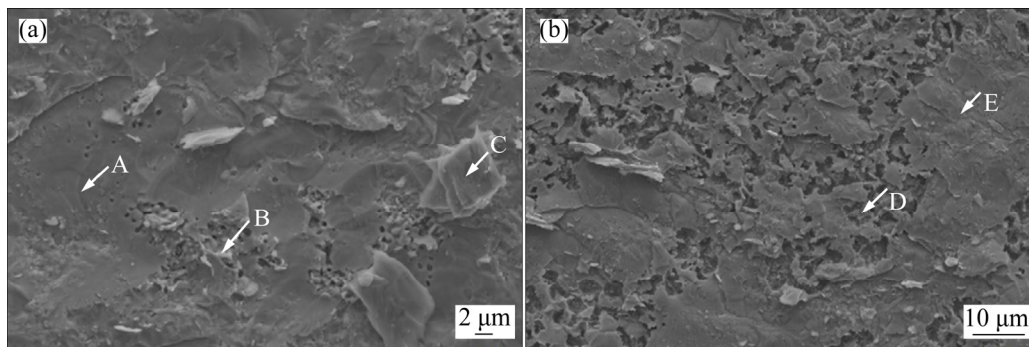


Fig. 9 Fracture morphology of joint brazed at 1020 °C for 10 min on TiAl alloy side (a) and on 316L stainless steel side (b)

Table 3 EDS point analysis results of locations in Fig. 9 (at.%)

Location	Ti	Zr	Cu	Ni	Fe	Cr	Al	Possible phase
A	4.1	33.3	7.8	4.4	39.9	5.7	4.6	Laves- Fe_2Zr
B	4.7	27.4	1.7	9.9	49.5	6.0	0.8	Laves- Fe_2Zr
C	2.5	33.9	16.6	5.9	28.6	4.8	7.7	$\text{Cu}_9\text{Zr}_{11} + \text{Fe}_{23}\text{Zr}_6$
D	1.4	23.9	2.6	8.1	53.3	9.4	1.3	Laves- Fe_2Zr
E	0.7	7.2	1.2	5.1	63.7	22.1	–	$\alpha\text{-(Fe,Cr)}$

4 Conclusions

(1) Sound joints between TiAl alloy and 316L stainless steel can be obtained with Zr-based filler metal. The brazed seam can be divided into three layers including two diffusion layers and one residual filler layer. The typical microstructure of the brazed joint is TiAl alloy substrate/ α_2 -(Ti₃Al)/AlCuTi/residual filler metal/Cu₉Zr₁₁+Fe₂₃Zr₆/Laves-Fe₂Zr/ α -(Fe, Cr)/316L stainless steel substrate.

(2) The shear strength of brazed joints increases firstly and then decreases with increasing the brazing time and brazing temperature. The maximum shear strength of joint reaches 129 MPa at 1020 °C for 10 min.

(3) Lots of facets and voids on the fracture surface suggest the brittle fracture mode of the TiAl/316L SS brazed joint, and the Laves-Fe₂Zr layer is the weak point of the resultant joints.

(4) The growth kinetics of α_2 -(Ti₃Al) layer and the α -(Fe, Cr) layer can be described as $W = 3.639 \times 10^{-6} \sqrt{t} \exp\left(\frac{-195.769}{RT}\right)$ for the α_2 -(Ti₃Al) layer, and $W = 7.502 \times 10^{-10} \sqrt{t} \exp\left(\frac{-112.420}{RT}\right)$ for the α -(Fe, Cr) layer.

Acknowledgments

This work was financially supported by the National Natural Science Foundation of China (No. 51674060) and Collaborative Innovation Center of Major Machine Manufacturing in Liaoning province, China.

References

- [1] CHU Qiao-ling, BAI Rui-xiang, ZHANG Min, LI Ji-hong, LEI Zhen-kun, HU Ning, BELL J M, YAN Cheng. Microstructure and mechanical properties of titanium/steel bimetallic joints [J]. Mater Characterization, 2017, 132: 330–337.
- [2] BANERJEE D, WILLIAMS J C. Perspectives on titanium science and technology [J]. Acta Materialia, 2013, 61(3): 844–879.
- [3] BOYER R R, BRIGGS R D. The use of β titanium alloys in the aerospace industry [J]. Journal of Materials Engineering and Performance, 2005, 14(6): 681–685.
- [4] ASM Handbook. Vol. 3: Alloy phase diagrams [M]. ASM International, 1992.
- [5] LI Peng, LI Jing-long, SALMAN M, LIANG Li, XIONG Jiang-tao, ZHANG Fu-sheng. Effect of friction time on mechanical and metallurgical properties of continuous drive friction welded Ti6Al4V/SUS321 joints [J]. Materials and Design, 2014, 56: 649–656.
- [6] DONG Hong-gang, YU Lian-zhen, GAO Hong-ming, DENG De-wei, ZHOU Wen-long, DONG Chuang. Microstructure and mechanical properties of friction welds between TiAl alloy and 40Cr steel rods [J]. Transactions of Nonferrous Metals Society of China, 2014, 24(10): 3126–3133.
- [7] HAO Xiao-hu, DONG Hong-gang, LI Peng, XIA Yue-qing. Dissimilar joining of TC4 alloy to ST16 steel by GTAW [J]. Journal of Manufacturing Processes, 2019, 37: 413–417.
- [8] CHU Qiao-ling, ZHANG Min, LI Ji-hong, YAN Cheng, QIN Zhan-ling. Influence of vanadium filler on the properties of titanium and steel TIG welded joints [J]. Journal of Materials Processing Technology, 2017, 240: 293–304.
- [9] JING Yong-juan, YUE Xi-shan, GAO Xing-qiang, SU Di-yao, HOU Jin-bao. The influence of Zr content on the performance of TiZrCuNi brazing filler [J]. Materials Science & Engineering A, 2016, 678: 190–196.
- [10] LEE J G, HONG S J, LEE M K, RHEE C K. High strength bonding of titanium to stainless steel using an Ag interlayer [J]. Journal of Nuclear Materials, 2009, 395: 145–149.
- [11] LEE M K, PARK J J, LEE G J, KIM D W, LIM C H, RHEE C K, LEE Y B, LEE J K, HONG S J. Corrosion of Ti-STSS dissimilar joints brazed by a Ag interlayer and Ag–Cu–(Pd) alloy fillers [J]. Journal of Nuclear Materials, 2011, 409: 183–187.
- [12] LEE J G, LEE M K. Microstructure and mechanical behavior of a titanium-to-stainless steel dissimilar joint brazed with Ag–Cu alloy filler and an Ag interlayer [J]. Materials Characterization, 2017, 129: 98–103.
- [13] NODA T, SHIMIZU T, OKABE M, IIKUBO T. Joining of TiAl and steels by induction brazing [J]. Materials Science & Engineering A, 1997, 239–240: 613–618.
- [14] DONG Dan-dan, DONG Chuang. Composition interpretation procedure of bulk metallic glasses via example of Cu₆₄Zr₃₆ [J]. Journal of Non-Crystalline Solids, 2017, 460: 125–129.
- [15] TAKEUCHI A, INOUE A. Classification of bulk metallic glasses by atomic size difference, heat of mixing and period of constituent elements and its application to characterization of the main alloying element [J]. Materials Transactions, 2005, 46(12): 2817–2829.
- [16] XIA Yue-qing, LI Peng, HAO Xiao-hu, DONG Hong-gang. Interfacial microstructure and mechanical property of TC4 titanium alloy/316L stainless steel joint brazed with Ti–Zr–Cu–Ni–V amorphous filler metal [J]. Journal of Manufacturing Processes, 2018, 35: 382–395.
- [17] LI Yu-long, HE Peng, FENG Ji-cai. Interface structure and mechanical properties of the TiAl/42CrMo steel joint vacuum brazed with Ag–Cu/Ti/Ag–Cu filler metal [J]. Scripta Materialia, 2006, 55(2): 171–174.
- [18] RABAHI L, GALLOWAY M, GRASDIDIER T, BRADAI D, KELLOU A. Energetic of atomic hydrogen absorption in C15-Fe₂Zr Laves phases with ternary additions: A DFT study [J]. International Journal of Hydrogen Energy, 2017, 42(4): 2157–2166.

- [19] JIN Xiao-jie, CHEN Sheng-hu, RONG Li-jian. Effect of Fe_2Zr phase on the mechanical properties and fracture behavior of Fe–Cr–W–Zr ferritic alloy [J]. Materials Science & Engineering A, 2018, 722: 173–181.
- [20] LI Peng, PAN Long-wei, HAO Xiao-hu, LI Shuai, DONG Hong-gang. Effect of post-weld heat treatment on inhomogeneity of aluminum–copper rotary friction welded joint [J]. Materials Research Express, 2018, 5(9): 096504. DOI:10.1088/2053-1591/aad58b
- [21] LI Yu-long, LIU Wen, HE Peng, FENG Ji-cai, SEKULIC D P. Dissolution of TiAl alloy during high temperature brazing [J]. Journal of Materials Science, 2013, 48: 5247–5252.

Zr–Cu–Ni–Al 非晶钎料钎焊 TiAl 合金/316L 不锈钢接头的界面特征

董红刚, 张润泽, 夏月庆, 郝晓虎, 李 鹏

大连理工大学 材料科学与工程学院, 大连 116024

摘 要: 采用 Zr–50.0Cu–7.1Ni–7.1Al (摩尔分数, %)非晶钎料钎焊 TiAl 合金/316L 不锈钢, 并针对钎焊时间和温度对接头界面显微组织与剪切强度的影响进行研究。钎缝由两个扩散层和一个中间的残留钎料层组成。TiAl 合金/316L 不锈钢钎焊接头的典型结构为: TiAl 合金母材/ α_2 -(Ti₃Al)/AlCuTi/残留钎料层/ $\text{Cu}_9\text{Zr}_{11}+\text{Fe}_{23}\text{Zr}_6$ /Laves- $\text{Fe}_2\text{Zr}/\alpha$ -(Fe,Cr)/316L 不锈钢母材, 在残留钎料层和 α -(Fe,Cr)层之间存在不连续的脆性 Fe_2Zr Laves 相。钎焊参数为 1020 °C、10 min 时接头剪切强度达到最大值 129 MPa。 α_2 -(Ti₃Al)相和 α -(Fe,Cr)相的生长激活能分别为–195.769 和–112.420 kJ/mol, 其扩散常数分别为 3.639×10^{-6} 和 $7.502\times 10^{-10} \mu\text{m}^2/\text{s}$ 。断口分析结果显示, 裂纹在 Fe_2Zr 层中萌生, 然后向残留钎料层扩展, 断口呈现脆性断裂特征且在断口表面检测到 Fe_2Zr Laves 相。

关键词: 真空钎焊; 异种金属焊接; Zr 基非晶钎料; 金属间化合物; 生长动力学

(Edited by Xiang-qun LI)